NACA

RESEARCH MEMORANDUM

EFFECT OF A REDUCTION IN STATOR SOLIDITY ON PERFORMANCE OF A TRANSONIC TURBINE

By James W. Miser, Warner L. Stewart, and Robert Y. Wong

Lewis Flight Propulsion Laboratory
Cleveland, Ohio

NATIONAL ADVISORY COMMITTEE FOR AERONAUTICS

WASHINGTON

March 23, 1956
Declassified December 3, 1958

NATIONAL ADVISORY COMMITTEE FOR AERONAUTICS

RESEARCH MEMORANDUM

EFFECT OF A REDUCTION IN STATOR SOLIDITY ON PERFORMANCE OF A TRANSONIC TURBINE

By James W. Miser, Warner L. Stewart, and Robert Y. Wong

SUMMARY

In order to determine the effect on turbine performance of a reduction in stator solidity and at the same time maintaining zero suction-surface diffusion, a transonic turbine with a highly loaded zero-suction-surface-diffusion stator was investigated experimentally. The performance results of the turbine show that the total-pressure-ratio adiabatic efficiency of the turbine is 0.869 at design specific work and design speed. A comparison of the subject turbine with a turbine using the same rotor but a lighter-loaded stator with a 25-percent-higher solidity indicated that at design point the efficiencies were the same within experimental accuracy, the maximum efficiencies of the two turbines were the same, and the mean-section blade-loss characteristics were about the same over the range of blade-outlet velocities investigated.

A three-dimensional design procedure previously used on low-reaction rotors was adapted for stators. The new procedure appeared to be satisfactory for maintaining zero suction-surface diffusion.

INTRODUCTION

Although turbine losses attributable to stators are not normally as high as those of rotors, any reduction of turbine losses by changing stator design characteristics is important. One blade characteristic that directly affects the over-all loss is solidity. It would be expected that a reduction in stator solidity would decrease the turbine losses up to a certain stator-blade-loading condition, and beyond this condition suction-surface-diffusion losses would more than offset the reduction in losses attributable to a change in solidity. Therefore, the effect on turbine performance of increasing the stator-blade loading by reducing the solidity and at the same time maintaining zero suction-surface diffusion by design techniques established for highly loaded low-reaction rotors (refs. 1 and 2) was investigated. This was done by comparing the performance of a turbine using the subject stator with the performance of a turbine using the

same rotor and the same design conditions but with the stator of reference 3. The results of this investigation are reported herein on the basis of turbine over-all efficiency, annular-survey results, and blade-loss characteristics.

DESIGN

Design Requirements

The design requirements for the 14-inch cold-air turbine investigated are nominally the same as those for the reference transonic turbines, which are as follows:

Equivalent specific work output, $\Delta h'/\theta_{cr}$, Btu/lb	22.61
Equivalent weight flow, $\frac{\varepsilon w\sqrt{\theta_{cr}}}{\zeta}$, lb/sec	11.95
Equivalent tip speed, $U_t/\sqrt{\theta_{cr}}$, ft/sec	597

The symbols used in this report are defined in appendix A.

Rotor Design

The rotor used for this investigation is the most efficient transonic-turbine rotor that has been investigated in the present program. For the details of its design see reference 4.

Design Velocity Diagrams

The design velocity diagrams for the stator and rotor are the same as those of reference 4, except that the velocity diagrams at station 2 just inside the stator trailing edge are changed because of a reduced trailing-edge blockage. The new blockage at station 2 is based on 20 blades with 0.010-inch-thick trailing edges instead of 32 blades with 0.010-inch-thick trailing edges. The new stator velocity diagrams are shown in figure 1.

Stator Design Assumptions

The assumptions used to determine the stator velocity diagrams are (1) free-vortex flow out of the stator, (2) simple radial equilibrium

throughout the stator, and (3) total pressure at stator exit and at channel exit (stations 3 and 1, respectively, in fig. 1) equal to 0.97 of stator-inlet total pressure.

Stator Design Considerations

In order to increase the stator-blade loading without introducing other factors that would affect turbine performance, a selection of the desirable maximum loading had to be made. This selection was based on a surface velocity distribution that indicated high velocities with zero diffusion on the suction surface and low velocities on the pressure surface limited by a reasonable blade thickness. The zero-suction-surface-diffusion limit was specified on the basis of the results of the reference transonic-turbine rotors, which showed that any amount of suction-surface diffusion is apparently detrimental, especially at the velocity levels along the suction surface of transonic-turbine stators and rotors. Figure 3 shows that, even with these suction-surface velocity limitations, high blade loading was achieved by making the suction-surface velocity equal to the blade-exit velocity over much of the suction-surface length and decreasing the pressure-surface velocity as much as possible while still maintaining a blade of reasonable thickness as shown in figure 2(a). In order that a comparison can be made of the loading of the subject stator with that of the stator of reference 3, the surface velocity distributions for the two stators are plotted against the blade-surface length ratio x/l in figure 4. The difference in the areas enclosed by the curves of surface velocity distribution of both stators approximates the difference in the blade loading. As shown in figure 4, the loading of the subject stator is considerably greater than that of the reference stator.

Stator Design Procedure

In order to control the surface velocities the three-dimensional rotor design procedure of reference 2 with the changes outlined in reference 1 was adapted for use on stators. In this procedure continuity across the stator and equilibrium in the radial-axial plane at each axial station had to be satisfied. The satisfaction of these two conditions plus meeting the assumed requirement of zero suction-surface diffusion made the design procedure an iterative one. Because the present stator design procedure is slightly different from that given in references 1 and 2, it is rewritten with the changes required as follows:

(1) A blade shape (fig. 2(a)) was first approximated as follows:

(a) A solidity was selected that was considered to be much lower than that of the stator of reference 3.

(b) A straight suction surface from the channel exit to the trailing edge was drawn at an angle equal to the exit flow angle α_3.

(c) The suction surface was then drawn from the channel exit to the approximate leading edge with low curvature near the channel exit and high curvature near the leading edge.

(d) At a distance of 1 blade spacing away from the suction surface, the pressure surface was drawn from the trailing edge to the approximate leading edge with very low curvature along the entire surface except for a short length near the leading edge.

(2) A first approximation of the suction-surface velocity was assumed equal to the blade-outlet velocity along the entire length of the suction surface at the hub, mean, and tip.

(3) The pressure-surface and midchannel velocity distributions were obtained from step (2) by the method given in appendix B.

(4) The blade surfaces were then adjusted until smooth midchannel and pressure-surface velocity-distribution curves resulted at each section.

(5) Using the resulting midchannel velocity distribution at the tip, the blade shape was then analyzed to obtain the midchannel velocities at the hub and mean at each axial station that must exist to satisfy simple-radial-equilibrium conditions. The procedure used to obtain the midchannel velocity variation from tip to hub is given in appendix B.

(6) The midchannel velocities obtained in step (5) were then used to recompute the surface velocity distributions at the hub and mean.

(7) The weight flow across each orthogonal surface (fig. 5) from the inlet to the channel exit was then calculated from the surface velocities at the hub, mean, and tip by the method given in appendix B.

(8) If the calculated weight flow across each orthogonal surface did not agree with the design weight flow, the originally assumed suction-surface velocity distribution at the tip was changed and the steps repeated until the design weight flow across each orthogonal surface was obtained. Then the surface velocity distributions at each blade section were analyzed with regard to diffusion and blade loading.

(9) If the velocity distributions and blade loading of step (8) did not meet the conditions discussed in Stator Design Considerations, the blade shape was altered until the conditions of radial equilibrium, continuity, zero suction-surface diffusion, high blade loading, and almost zero incidence angle were satisfied.

(10) In step (1d) the trailing edge was assumed to be of zero thickness; therefore, a finite trailing-edge thickness of 0.010 inch was added on the suction-surface side of the blade, and a straight line was drawn

tangent to the trailing-edge circle and the suction surface near the channel exit.

Because the resulting trailing-edge blockage was so small, no change was made elsewhere on the blade. The resulting blade-section profiles obtained in the preceding steps are shown in figure 2(a). The coordinates of each blade section are given in table I. For comparison, the blade-section passages and profiles of the stator of reference 3 are reprinted in this report in figure 2(b).

(11) In order to obtain the final blade shape the stator-blade profiles for the hub, mean, and tip were stacked so that the centers of the channel exits for all three sections were on a radial line.

Discussion of Stator Design

As shown in figure 3 the suction-surface velocities within 1/2 inch of the leading edge drop below a critical-velocity ratio of 0.8 for each blade section. The reason for this is that the suction-surface curvature was not made too high near the leading edge in order that the pressure and suction surfaces would not diverge rapidly at the leading edge and result in a high incidence angle for the pressure surface.

It should be noted in figure 3 that, of the three blade sections, the tip is the most critical with respect to diffusion because of the lower reaction; therefore, the suction-surface curvature in the region just upstream of the channel exit could not be as high at the tip as it was at the hub. Even so, the suction-surface length from the leading edge to the channel exit is approximately 1.2 inches for all three sections, because the required turning decreases from 66.3° at the hub to 58.1° at the tip.

The method used for designing the blade sections resulted in a variation in the suction-surface length downstream of the channel exit from hub to tip. In figures 3(a) and (c) this length is only 1.4 inches at the hub and 1.9 inches at the tip, respectively.

The three-dimensional design procedure outlined had been previously used only on low-reaction highly loaded rotors; therefore, it was interesting to see how well the procedure could be applied to high-reaction stators such as the subject one. It is felt that good accuracy in predicting the surface velocities near the channel exit was obtained, but toward the leading edge the validity of the surface velocity predictions became more questionable, mainly because of the increase in the orthogonal length and the arbitrariness in locating the orthogonal end points on the surfaces. However, a check of the circulation around the channel from the

leading edge to the channel exit showed that the calculated circulation was almost 0 for each blade section; therefore, it can be assumed that the velocity distributions are approximately correct. Because the blade wrapped around the annulus about 22°, considerable error would have been introduced by assuming that the blade design sections were flat in making templates for blade fabrication. Therefore, a special means had to be devised for obtaining coordinates for flat templates from the design blade sections that actually described the profiles of cylindrical cross sections of the blade. A special transformation for obtaining the flat-template coordinates is discussed in appendix C.

APPARATUS, INSTRUMENTATION, AND PROCEDURE

The apparatus, instrumentation, and procedure for calculating the turbine performance parameters are the same as those described in reference 2 and used for the turbines of references 1 to 5. A diagrammatic sketch of the cold-air-turbine test rig is shown in figure 6.

For turbine performance tests the rotor was operated at 60, 70, 80, 90, 100, 110, 120, and 130 percent of design speed. For each speed the total-pressure ratio was varied from approximately 1.4 to the maximum pressure ratio obtainable. Turbine-inlet conditions were maintained constant at nominal values of 145° F and 32 inches of mercury absolute.

In order to study the operating characteristics of the stator, tests were made with and without the rotor in place. Radial and circumferential surveys of total pressure, total temperature, and angle were taken at design conditions at station 6 (fig. 6) with the rotor in place. At station 3 just downstream of the stator trailing edge, annular surveys of total pressure and angle were made at design conditions and at one off-design point at an exit Mach number lower than the design value to determine the total-pressure and angle variations behind the stator. Also, for different blade-exit total- to static-pressure ratios, mean-section surveys were made to determine the total-pressure profile of the blade wake within 0.003 inch axially of the stator trailing edge.

RESULTS AND DISCUSSION

Performance Results

The over-all performance of the subject transonic turbine is presented in figure 7, which shows the equivalent specific work output $\Delta h'/\Theta_{cr}$ as a function of the weight-flow - speed parameter $\epsilon wN/\zeta$ for the various percentages of design speed. Also shown on the performance map are contours of total-pressure-ratio adiabatic efficiency η. As shown by

figure 7 the efficiency at design work and speed is 0.869 and the maximum efficiency is 0.878.

An investigation of the same turbine rotor as used in the subject investigation with a stator of 25-percent-higher solidity is discussed in reference 3. The performance map of the reference turbine is given in figure 8 in order that comparisons can be made with the subject turbine in studying the effect of a reduction in stator solidity on turbine performance. The efficiency η at design specific work and speed of the reference turbine was 0.872, and the maximum efficiency was 0.878. Thus, the design-point efficiency of the subject turbine was only 0.003 less than that of the reference turbine, which is within experimental accuracy; and their maximum efficiencies were the same. This indicates that the reduction in stator solidity had little effect on the design-point performance.

The efficiencies of the subject turbine at off-design conditions are generally not quite as high as those for the reference turbine, but the difference between the efficiencies for the two turbines at a particular speed and work does not exceed 0.02 over the entire map.

Stator Survey Results

The results of detailed total-pressure surveys downstream of the stator trailing edge are shown in figure 9 as contours of constant total pressure. The pressure loss along the stator trailing edge is fairly large, but the loss region at the intersection of the suction surface and the hub is even larger. In order to compare these loss regions with those of the previously investigated stator of reference 3, the total-pressure-survey results of the latter are given in figure 10. For the subject stator the loss region at the hub spreads over almost three-fourths of the blade spacing as compared with this same loss region of the reference stator which extends over about one-third of its blade spacing. The width of the wake at the mean section of each blade of the subject stator is about twice that of each blade of the reference stator. These comparisons indicate that as the stator-blade loading increases the wake becomes larger for each blade. However, counteracting the effect of the increased size of the wake is the increased size of the free stream between blade wakes. Therefore, the increased blade loading did not greatly affect the percentage of free-stream area around the entire annulus downstream of the stator. This partially explains why the efficiencies at design point for the subject turbine and the turbine of reference 3 are approximately the same.

Rotor Survey Results

The results of the radial and circumferential surveys of total temperature and pressure made downstream of the rotor trailing edge with the turbine set at design work and speed are shown in figure 11 as contours of constant local adiabatic efficiency η_l. An analysis of similar rotor surveys discussed in reference 6 compares the rotor survey results of the transonic turbines of references 1 and 5. As shown by reference 6 the rotor effects are indicated to some extent by the maximum value taken in a circumferential direction at a given radius and stator effects by the minimum value. Therefore, the effects of the stator wakes are distinguishable from rotor effects in the surveys downstream of the rotor. For this reason the regions of low efficiency in figure 11 represent some of the effects of stator wakes on the rotor. For instance, the large loss region at the upper right corner is attributed to a large stator wake region coming through the rotor. The loss region running diagonally across the lower left corner of figure 11 may also be an effect of the stator trailing-edge wake.

In order to compare the local efficiency contours of the subject turbine with those of reference 3, figure 5(a) of reference 3 is reprinted as figure 12 in this report. The loss regions for the reference turbine are similar in location but smaller in size than those for the subject turbine. However, considering the difference in the spacing between stator wakes for the two turbines resulting from the differences in the number of stator blades, the location of the contours of high and low local efficiency can be considered as very similar. Nevertheless, a slight difference between the local efficiency contours can be found by examining the radial variation in maximum and minimum local efficiencies given in figure 13. This figure indicates that the average between the maximum and minimum curves is about the same for the two turbines; however, the minimum curve of the subject turbine is on the average somewhat lower than that of the reference turbine, and the maximum curve for the subject turbine is on the average somewhat higher than that of the reference turbine. As shown in figures 9 and 10, the size of each blade wake is considerably larger for the subject stator than for the reference stator, expecially near the hub; therefore, considering that the stator wakes are incompletely mixed at the measuring station behind the rotor, the subject turbine with the larger stator wake would be expected to have a correspondingly lower minimum local efficiency. This trend is shown in figure 13 from the hub to the mean, but is not apparent near the tip.

The high local efficiencies near the hub in figure 11 show that very little hub boundary layer is present at the rotor exit. The local efficiencies near the tip indicate that there is a thicker boundary layer at

the tip than at the hub; but, with the exception of the large loss region attributable to the stator wake, the hub and tip boundary layers are small.

Stator-Blade Loss

In reference 7 the boundary-layer parameters at the mean section of the subject stator were calculated from experimental survey data at the mean section. The momentum-thickness to chord ratios θ_{tot}/c for different values of outlet free-stream critical-velocity ratio $(V/V_{cr})_{fs,2}$ are shown in figure 14(a). Similar values for the stator of reference 3 were calculated for figure 4 of reference 8, and these values are presented again in figure 14(b) of this report. The trend of decreasing momentum thickness as the exit velocity increases can be seen in both figures 14(a) and (b). At the design value of $(V/V_{cr})_{fs,2} = 1.107$, the θ_{tot}/c for the subject stator is 0.0033 and for the reference 32-blade stator θ_{tot}/c is 0.0032; therefore, the average rate of boundary-layer build-up along the blade surface is about the same for the two stators.

In reference 8, which presents a study of mean-section boundary-layer characteristics for the stator of reference 3, the momentum-thickness to chord ratios for the suction and pressure surfaces were calculated for different exit velocities. Similarly, momentum-thickness to chord ratios were calculated for the pressure and suction surfaces of the subject stator. The values for the subject stator are shown in figure 15(a), and those for the reference stator are given again in figure 15(b). The values of the suction-surface momentum-thickness to chord ratio θ_s/c of the subject stator are higher than those of the reference stator; however, for the pressure surface the θ_p/c values are lower for the subject stator than those for the reference stator. Both trends might be predicted from a comparison of the velocity levels along the surfaces of the two blades (fig. 4). The more highly loaded stator of this report has higher velocities on the suction surface and lower velocities on the pressure surface than those of the reference stator, and the boundary-layer growth is a function of the velocity level (see ref. 8).

The form factors H_{tot} for the subject stator are presented in figure 16(a). The values of H_{tot} and the theoretical curve for H for the reference stator have previously been presented in figure 5 of reference 8 and are given again in figure 16(b) for comparison. As shown in figure 16 the form factor H_{tot} for both stators is higher than H for the theoretical simple-power-law velocity profile for

$n = 1/7$, which indicates that the displacement thickness is greater than that for the profile with an exponent of $n = 1/7$. Even though the form factor for the subject stator is slightly higher than that of the reference stator, it follows the same trend with increasing exit velocities; and at the design outlet free-stream critical-velocity ratio $(V/V_{cr})_{fs,2}$ of 1.1, the form factors of the two stators are almost identical.

The preceding comparison of the mean-section blade-loss characteristics of the two stators is good for the essentially two-dimensional flow at the mean section; however, a consideration of the three-dimensional loss taking into account the losses due to the inner and outer walls gives a more accurate determination of the total loss of each stator. A method for computing this three-dimensional loss from mean-section boundary-layer parameters is presented in reference 7. The total-pressure ratios presented in figure 8 of reference 7 are given again in figure 17. The two circled points in figure 17 are mass-averaged values of total-pressure ratio across the subject stator corrected for total-pressure loss upstream of the stator attributed to inlet boundary layer, and they are given here to show the agreement between the total-pressure ratio obtained by mass-averaging survey values and that obtained from mean-section boundary-layer parameters.

The total-pressure-ratio curve for the 32-blade stator of reference 3 was also calculated by the method given in reference 7. The curves in figure 17 for the two stators are smooth because they were obtained from curves faired through the scatter of points in figure 14. It should be noted that the two curves are almost identical, which indicates that similar performance might be expected for both. The fact that the reference stator performed slightly better than the subject stator is probably attributable to different types of interference effects on the rotor, which are not taken into account in studying stator losses in the method of reference 7.

SUMMARY OF RESULTS AND CONCLUDING REMARKS

In order to determine the effect on turbine performance of a reduction in stator-blade solidity and at the same time maintaining zero suction-surface diffusion, a transonic turbine with a highly loaded, zero-suction-surface-diffusion stator was investigated experimentally, with the following results:

1. At design equivalent specific work and design speed the total-pressure-ratio efficiency was 0.869.

1. At design equivalent specific work and design speed the total-pressure-ratio efficiency was 0.869.

2. A comparison of the performance of the subject turbine with that of the turbine of reference 3 with the same rotor but a lighter-loaded zero-suction-surface-diffusion stator with a 25-percent-greater solidity showed that the stator losses were about the same by the following results:

(a) At design point the subject turbine had an efficiency which was only 0.003 less than that of the reference turbine.

(b) The maximum efficiencies of the two turbines were the same (0.878).

(c) At off-design conditions the efficiency of the subject turbine was at most only 0.02 less than that of the reference turbine.

(d) The blade-loss characteristics of the two stators were about the same at design operating conditions.

This report shows that stator solidity can be reduced without penalizing turbine performance if zero duffusion is maintained on the suction surface. An effective means of maintaining zero suction-surface diffusion for stators is the three-dimensional design procedure previously used for low-reaction rotors.

Lewis Flight Propulsion Laboratory
National Advisory Committee for Aeronautics
Cleveland, Ohio, December 12, 1955

APPENDIX A

SYMBOLS

A	arc length from point on suction surface to a parallel to axis of rotation through center of channel exit (fig. 2(a)), ft
B	arc length from point on pressure surface to a parallel to axis of rotation through center of channel exit (figs. 2(a) and 18), ft
b	number of blades
C	curvature, ft^{-1}
c	chord length, ft
d	distance in direction normal to boundary-layer travel, ft
H	boundary-layer form factor, δ/θ; $H_{tot} = \delta^*/\theta^*$
$\Delta h'$	specific work output, Btu/lb
l	blade surface length, in.
l_o	orthogonal length, ft
N	rotational speed, rpm
n	exponent used in describing boundary-layer velocity profile, $\frac{V}{V_{fs}} = y^n$
P	pressure, lb/sq ft
r	radius, ft
s	blade spacing, ft
U	blade velocity, ft/sec
u	abscissa in radial plane of point on blade, ft
V	absolute gas velocity, ft/sec
v	ordinate in radial plane of point on blade, ft

w weight flow, lb/sec

x distance along surface from blade leading edge, in.

y distance in direction normal to boundary-layer travel in terms of δ_{full}, $y = d/\delta_{full}$

z radial distance from hub, ft

α gas-flow angle measured from axial direction, deg

γ ratio of specific heats

δ boundary-layer displacement thickness, ft

δ^* ratio of projection of total displacement thickness along a circumferential path to blade spacing, $(\delta_s + \delta_p)/(s \cos \alpha)$

δ_{full} full boundary-layer height, ft

ε $$\frac{\gamma_{sl}}{\gamma}\left[\frac{\left(\frac{\gamma+1}{2}\right)^{\frac{\gamma}{\gamma-1}}}{\left(\frac{\gamma_{sl}+1}{2}\right)^{\frac{\gamma_{sl}}{\gamma_{sl}-1}}}\right]$$

ζ ratio of inlet-air total pressure to NACA standard sea-level pressure, P'_0/P_{sl}

η total-pressure-ratio adiabatic efficiency defined as ratio of turbine work based on torque, weight flow, and speed measurements to ideal work based on inlet total temperature and inlet and outlet total pressure, both defined as sum of static pressure plus pressure corresponding to gas velocity

η_l local adiabatic efficiency based on total-state measurements from surveys downstream of rotor

Θ_{cr} squared ratio of critical velocity at turbine inlet to critical velocity at NACA standard sea-level temperature, $(V_{cr,0}/V_{cr,sl})^2$

θ boundary-layer momentum thickness, ft

θ^* momentum-thickness parameter defined as $(\theta_s + \theta_p)/(s \cos \alpha)$

ρ gas density, lb/cu ft

φ angle in radial plane describing point on blade (fig. 18), radians

Subscripts:

av average

cr conditions at Mach number of 1.0

fs conditions at free stream or that region between blade wakes

h hub

mid midchannel

p pressure surface

s suction surface

sl NACA standard sea-level conditions

t tip

tot sum of suction- and pressure-surface quantities

0 station upstream of stator (see fig. 1)

1 station at stator channel exit

2 station at outlet of stator just upstream of trailing edge

3 station at free-stream condition between stator and rotor

6 station downstream of turbine (see fig. 6)

Superscript:

' total state

APPENDIX B

CALCULATION METHODS

The following discussion presents equations and methods given in appendix B of reference 2 (with changes outlined in reference 1) adapted for use on stators.

Surface Velocity Distribution

By the simplified stream-filament theory of reference 9, the midchannel and suction- and pressure-surface velocity distributions can be calculated if one of the three velocity distributions is known or assumed. The calculation of the suction-surface velocity from an assumed midchannel velocity can be made by

$$\frac{V_s}{V_{mid}} = \exp\left[\frac{C_s l_o}{2}\left(1 + \frac{C_s - C_p}{4C_s}\right)\right] \tag{B1}$$

which is the same as equation (39) of reference 9 expressed in the symbols of this report. In equation (B1), C_s is the curvature of the suction surface at the end of the orthogonal, C_p is the curvature of the pressure surface at the end of the orthogonal, and l_o is the orthogonal length (fig. 5).

The calculation of the pressure-surface velocity from an assumed midchannel velocity can be made by

$$\frac{V_p}{V_{mid}} = \exp\left\{-\frac{C_s l_o}{2}\left[1 + \frac{3(C_s - C_p)}{4C_s}\right]\right\} \tag{B2}$$

which is the same as equation (40) of reference 9.

An alternate method of determining the values of equations (B1) and (B2) would be to use figures 17 and 18 of reference 9.

The curvatures C_s and C_p can be determined by a curvometer discussed in appendix B of reference 1.

Midchannel Velocity Distribution

The midchannel velocity-distribution calculations were based on the following assumptions: (1) axial symmetry exists, (2) there is negligible shift of streamline in the radial direction, (3) simple radial equilibrium exists, and (4) the flow follows an angle α_{av} which is the average of the angles of the pressure and suction surfaces measured from a parallel to the axis of rotation at either end of the orthogonal.

The radial variation of midchannel velocity can then be obtained by

$$V_{mid} = V_{mid,h}\, e^{\int_0^z \left(\frac{-\sin^2 \alpha_{av}}{r}\right) dz} \tag{B3}$$

where z equals the radial distance from the hub. This is similar to equation (B1) of reference 2; however, because there is no blade movement in the case of stators, one term of the equation is zero. In (B3) the angle α_{av} is the angle given by assumption (4).

With a known radial variation of midchannel velocity from hub to tip and solutions for equations (B1) and (B2) at each end of the orthogonal, the surface velocity distributions can be determined at all three blade sections for any assumed velocity distribution along one of the surfaces at either the hub, mean, or tip.

Weight Flow

Once the midchannel and surface velocity distributions are determined, the weight flow that passes through an orthogonal surface can be calculated from

$$w = b \int_{r_h}^{r_t} \int_0^{l_o} \rho V \, dl_o \, dr \tag{B4}$$

where b equals the number of blades. For the calculation of equation (B4), a linear variation in static pressure was assumed from pressure to suction surface along each orthogonal.

APPENDIX C

TRANSFORMATION OF CYLINDRICAL BLADE-DESIGN-SECTION COORDINATES TO COORDINATES OF PARALLEL TEMPLATES FOR BLADE FABRICATION

In the design of most conventional blades it is customary to design three or more blade sections. For short blades such as the subject stator (2.1 in. long radially), only the hub, mean, and tip design sections are usually required. For three-dimensional turbomachine blade rows the blade-design sections extend around cylindrical surfaces at the design radii (fig. 18). Usually, the amount the design sections wrap around the annulus is small, and the distortion incurred by assuming that the design sections are flat instead of cylindrical is insignificant. However, the subject stator wrapped around the annulus about 22°, and the distortion would have been large if the blade design sections had been assumed to be flat and stacked parallel to each other. Therefore, to eliminate the distortion, a transformation from the cylindrical coordinates of the blade sections to coordinates for flat templates perpendicular to the stacking line was developed with the use of automatic computing techniques.

The transformation of the coordinates is made as follows:

(1) A stacking point was selected for all three blade sections. For the subject turbine stator the stacking point was the center of the channel exit of each section (fig. 2(a)), and these points were stacked on a radial line.

(2) Equally spaced axial stations measured from the stacking point were located on each blade section.

(3) At each station the distances A and B (fig. 2(a)) from points on the suction and pressure surfaces to a line through the stacking point and parallel to the axis of rotation were read for each section. In order that there would be points on each section for each axial station, the suction and pressure surfaces were extended parallel to each other from the trailing edge and were faired upstream of the leading edge.

(4) Because the values of A and B are arc lengths measured along circles of the design-section radii and define a set of cylindrical coordinates. New Cartesian coordinates in a radial plane (fig. 18) were obtained from the equations

$$u_s = r \sin(A/r)$$

$$v_s = r \cos(A/r)$$

$$u_p = r \sin(B/r)$$

$$v_p = r \cos(B/r)$$

where A/r and B/r are values of φ in radians (fig. 18).

(5) At each axial station three points I, J, and K (fig. 18) were defined for the pressure surface by step (4); and similarly three points were defined for the suction surface. An equation for a parabola $u = f(v)$ through points I, J, and K was obtained by use of an automatic computing machine solving the general equation of a parabola through these three points. (For this stator a parabolic curve was used, but later work has shown that use of circular arcs would have been better. The reason is that cross sections of high curvature cause the vertex of the parabola to be too close to the blade, so that a parabolic arc would cause unusually high local curvatures.)

(6) For each plane perpendicular to the stacking line, a set of points defining a blade shape was obtained by substituting the v-values for each plane into the equation of step (5). The points on each plane were joined by a faired line, and a leading edge was faired to the desired leading-edge radius. The trailing edge was obtained from a plot of the projection of point D (fig. 2(a)) for each section on an axial plane through the stacking line. A new point D for each v-valued plane was then read from this plot, and this new point determined the point of tangency of the pressure surface and the trailing-edge circle for the new blade templates.

REFERENCES

1. Miser, James W., Stewart, Warner L., and Monroe, Daniel E.: Effect of High Rotor Pressure-Surface Diffusion on Performance of a Transonic Turbine. NACA RM E55H29a, 1955.

2. Stewart, Warner L., Wong, Robert Y., and Evans, David G.: Design and Experimental Investigation of Transonic Turbine with Slight Negative Reaction Across Rotor Hub. NACA RM E53L29a, 1954.

3. Whitney, Warren J., Stewart, Warner L., and Wong, Robert Y.: Effect of Reduced Stator-Blade Trailing-Edge Thickness on Over-All Performance of a Transonic Turbine. NACA RM E55H17, 1955.

4. Whitney, Warren J., Monroe, Daniel E., and Wong, Robert Y.: Investigation of Transonic Turbine Designed for Zero Diffusion of Suction-Surface Velocity. NACA RM E54F23, 1954.

5. Wong, Robert Y., Monroe, Daniel E., and Wintucky, William T.: Investigation of Effect of Increased Diffusion of Rotor-Blade Suction-Surface Velocity on Performance of Transonic Turbine. NACA RM E54F03, 1954.

6. Wong, Robert Y., Miser, James W., and Stewart, Warner L.: Qualitative Study of Flow Characteristics Through Single-Stage Turbines as Made from Rotor-Exit Surveys. NACA RM E55K21, 1956.

7. Stewart, Warner L., Whitney, Warren J., and Wong, Robert Y.: Use of Mean-Section Boundary-Layer Parameters in Predicting Three-Dimensional Turbine Stator Losses. NACA RM E55L12a, 1956.

8. Whitney, Warren J., Stewart, Warner L., and Miser, James W.: Experimental Investigation of Turbine Stator-Blade-Outlet Boundary-Layer Characteristics Compared with Theoretical Results. NACA RM E55K24, 1956.

9. Huppert, M. C., and MacGregor, Charles: Comparison Between Predicted and Observed Performance of Gas-Turbine Stator Blade Designed for Free-Vortex Flow. NACA TN 1810, 1949.

TABLE I. - STATOR-BLADE-SECTION COORDINATES

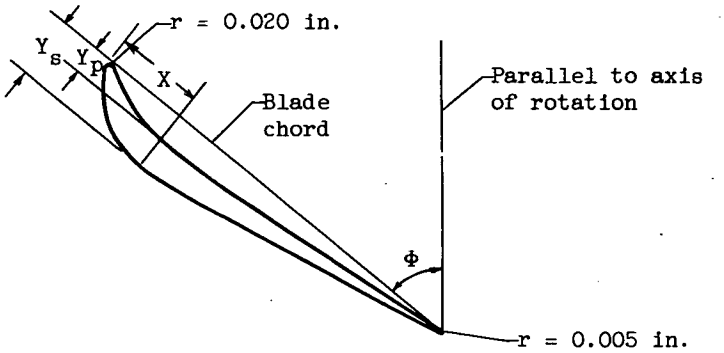

	Hub		Mean		Tip	
	Φ, deg					
	53.3		50.5		48.833	
	r/r_t					
	0.70		0.85		1.00	
X, in.	Y_s, in.	Y_p, in.	Y_s, in.	Y_p, in.	Y_s, in.	Y_p, in.
0	0.020	0.020	0.020	0.020	0.020	0.020
.10	.145	.060	.155	.052	.125	.048
.20	.232	.113	.247	.102	.207	.096
.30	.290	.148	.310	.136	.263	.124
.40	.331	.172	.353	.161	.304	.143
.50	.356	.185	.378	.176	.329	.152
.60	.370	.192	.390	.185	.342	.155
.70	.373	.195	.392	.187	.346	.155
.80	.367	.192	.384	.187	.342	.153
.90	.354	.189	.368	.184	.331	.148
1.00	.335	.184	.349	.179	.318	.145
1.10	.313	.176	.329	.174	.300	.141
1.20	.289	.168	.308	.167	.285	.136
1.30	.266	.158	.287	.161	.268	.132
1.40	.243	.147	.266	.153	.253	.128
1.50	.220	.136	.246	.145	.237	.122
1.60	.197	.125	.2255	.1375	.221	.117
1.70	.174	.112	.205	.129	.205	.110
1.80	.151	.100	.184	.119	.188	.104
1.90	.128	.087	.163	.108	.173	.098
2.00	.103	.071	.141	.096	.157	.091
2.10	.081	.057	.121	.085	.141	.084
2.20	.057	.040	.100	.070	.125	.076
2.30	.034	.021	.079	.056	.109	.068
2.40	.012	.000	.058	.041	.092	.059
2.407	.005	.005	----	----	----	----
2.50			.037	.024	.076	.050
2.60			.0165	.0055	.059	.040
2.632			.005	.005	----	----
2.70					.044	.027
2.80					.027	.015
2.90					.012	.002
2.918					.005	.005

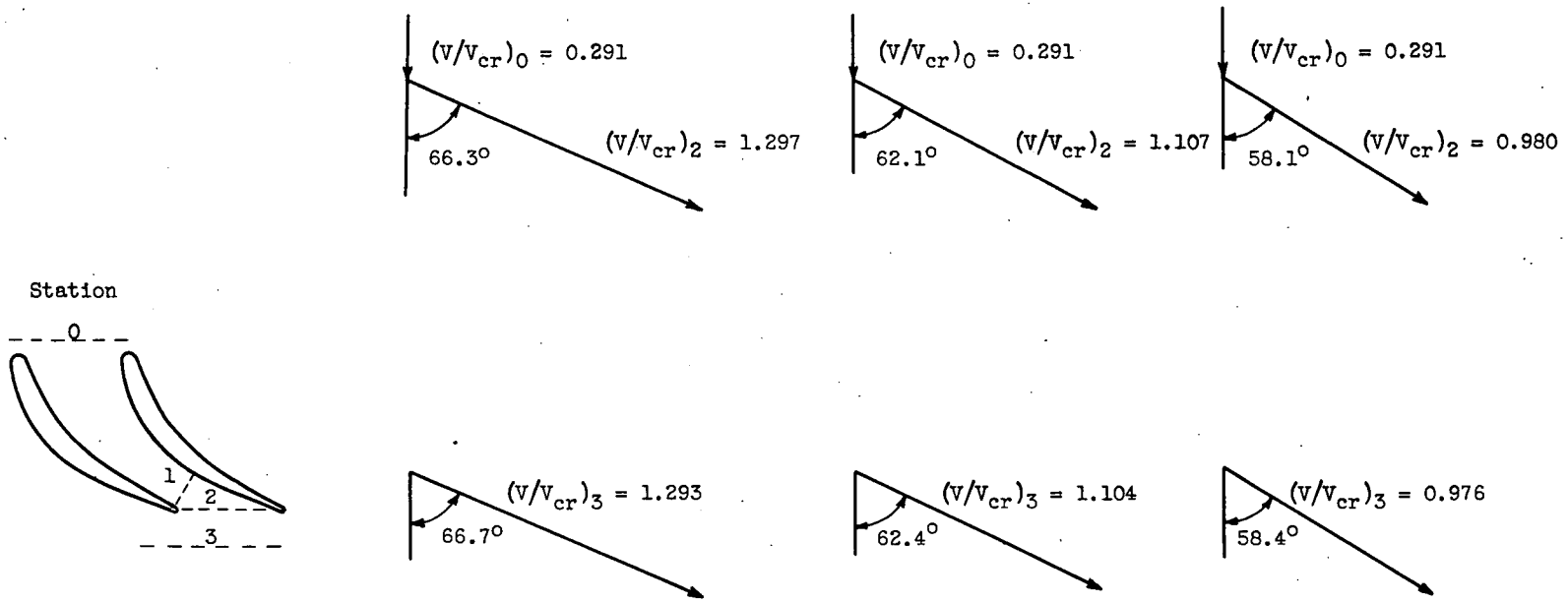

(a) Hub; r/r_t, 0.70. (b) Mean; r/r_t, 0.85. (c) Tip; r/r_t, 1.00.

Figure 1. - Transonic-turbine stator velocity diagrams.

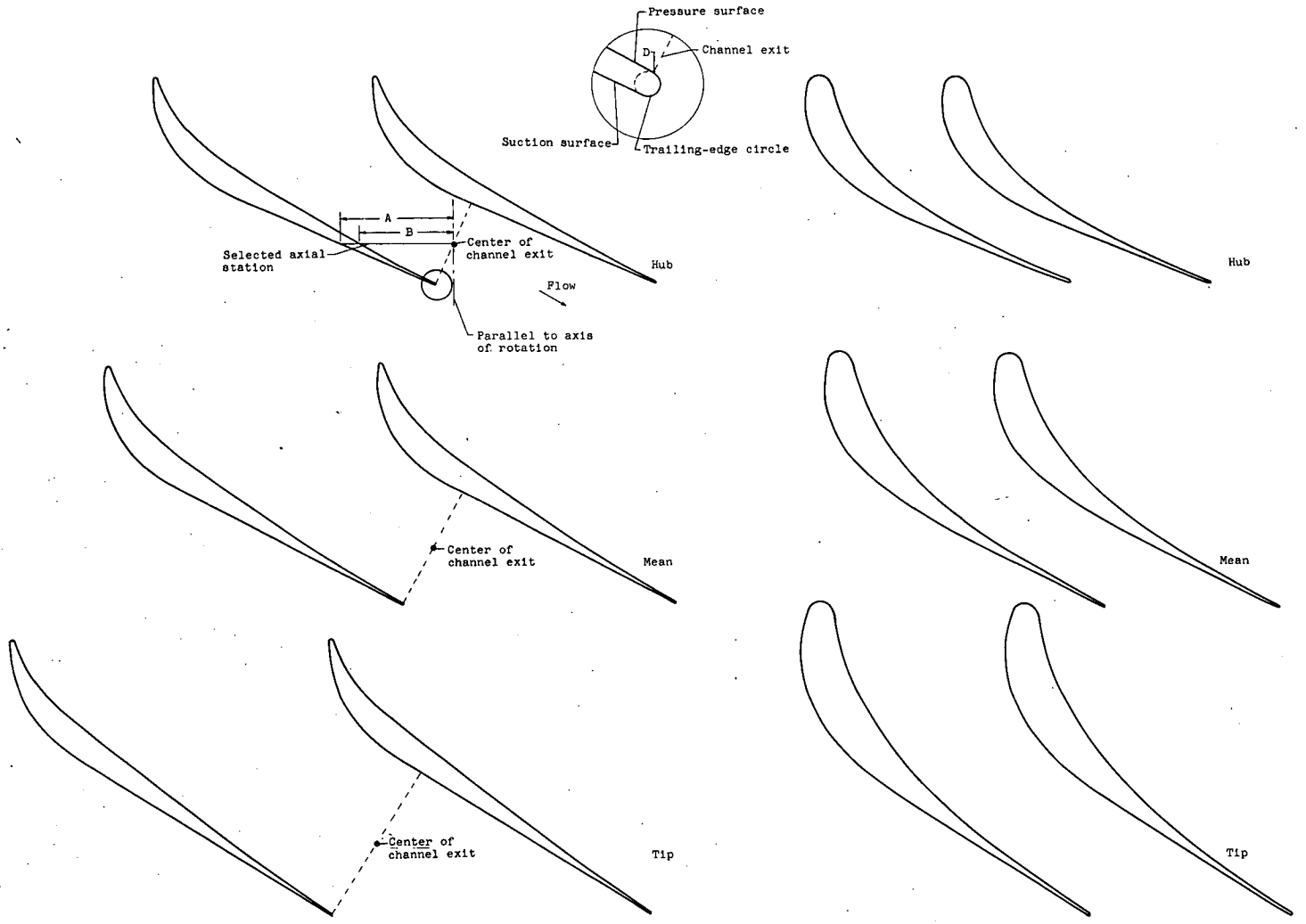

(a) Subject 20-blade stator.

(b) 32-Blade stator of reference 3.

Figure 2. - Stator-blade passages and profiles.

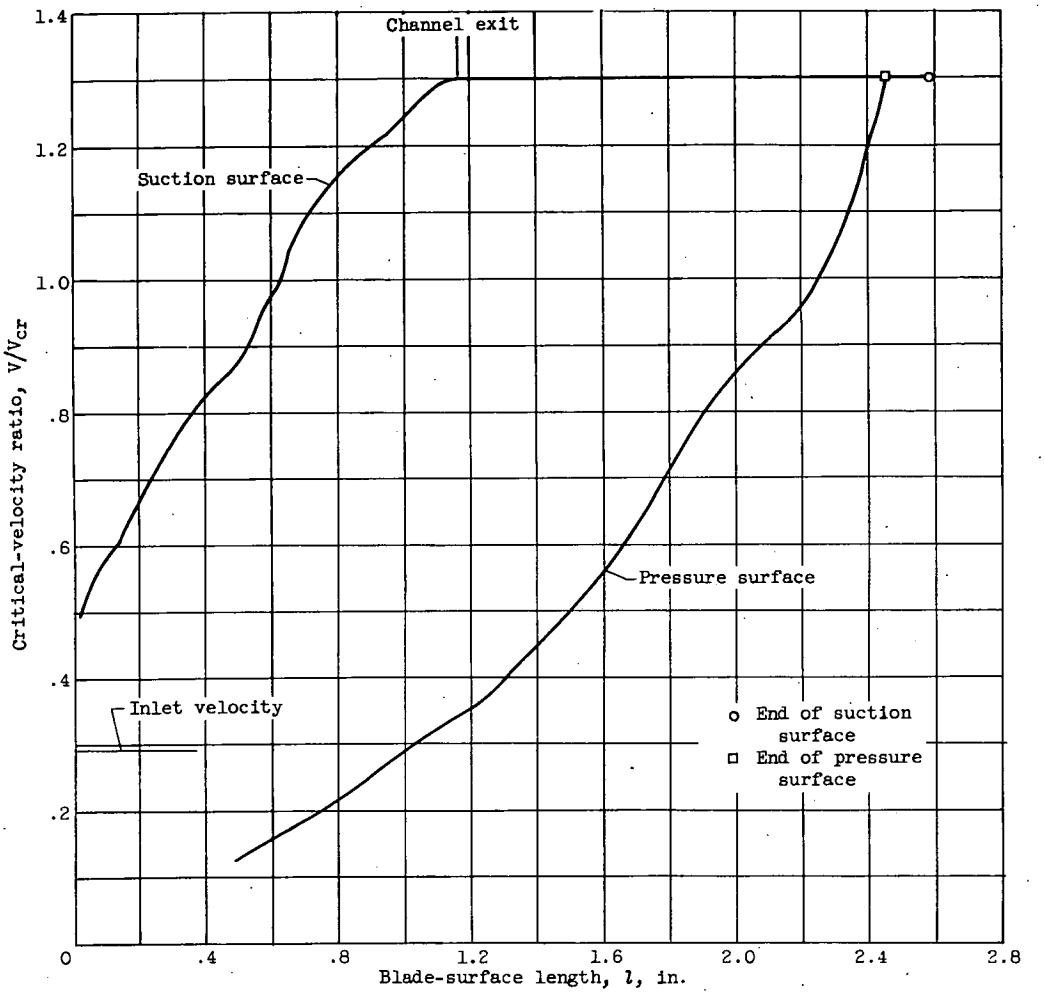

(a) Hub.

Figure 3. - Design stator-surface velocity distributions at hub, mean, and tip sections.

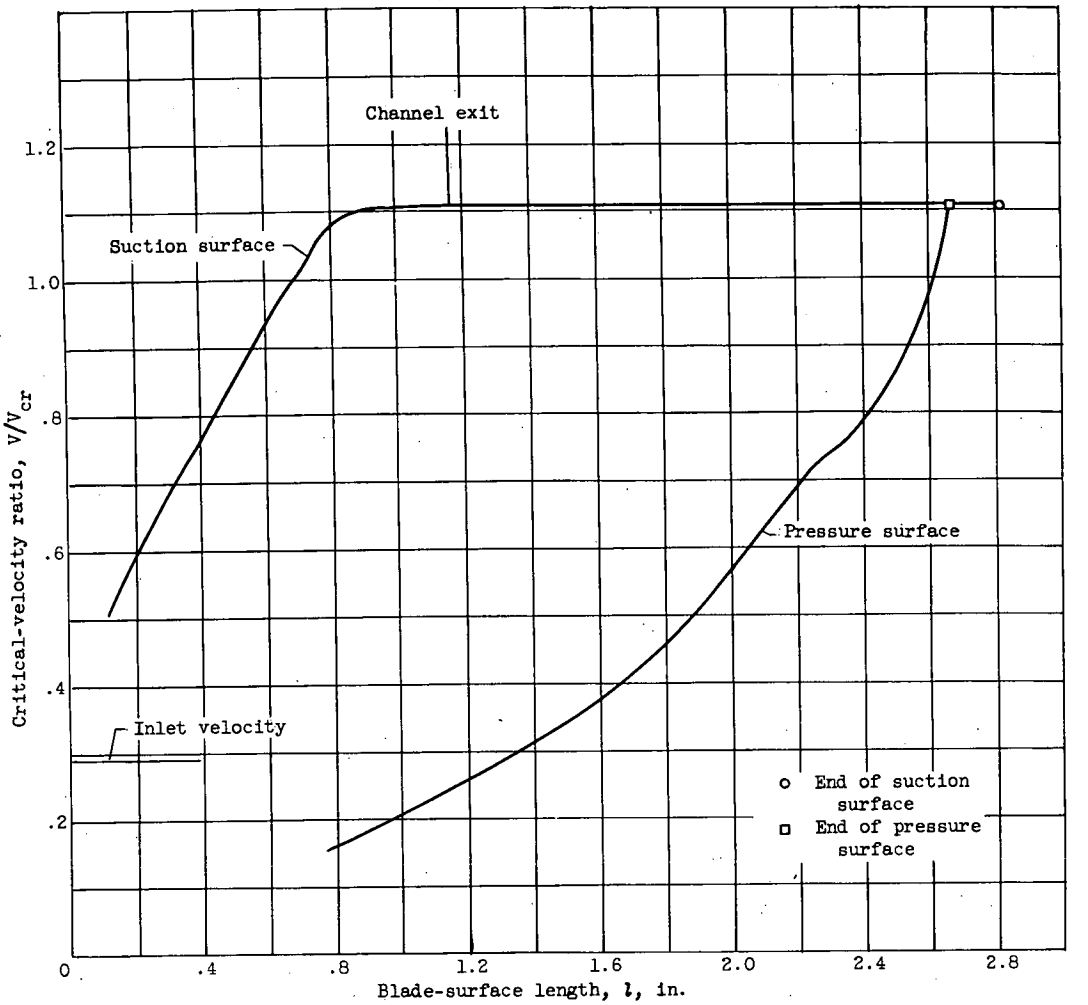

(b) Mean.

Figure 3. - Continued. Design stator-surface velocity distributions at hub, mean, and tip sections.

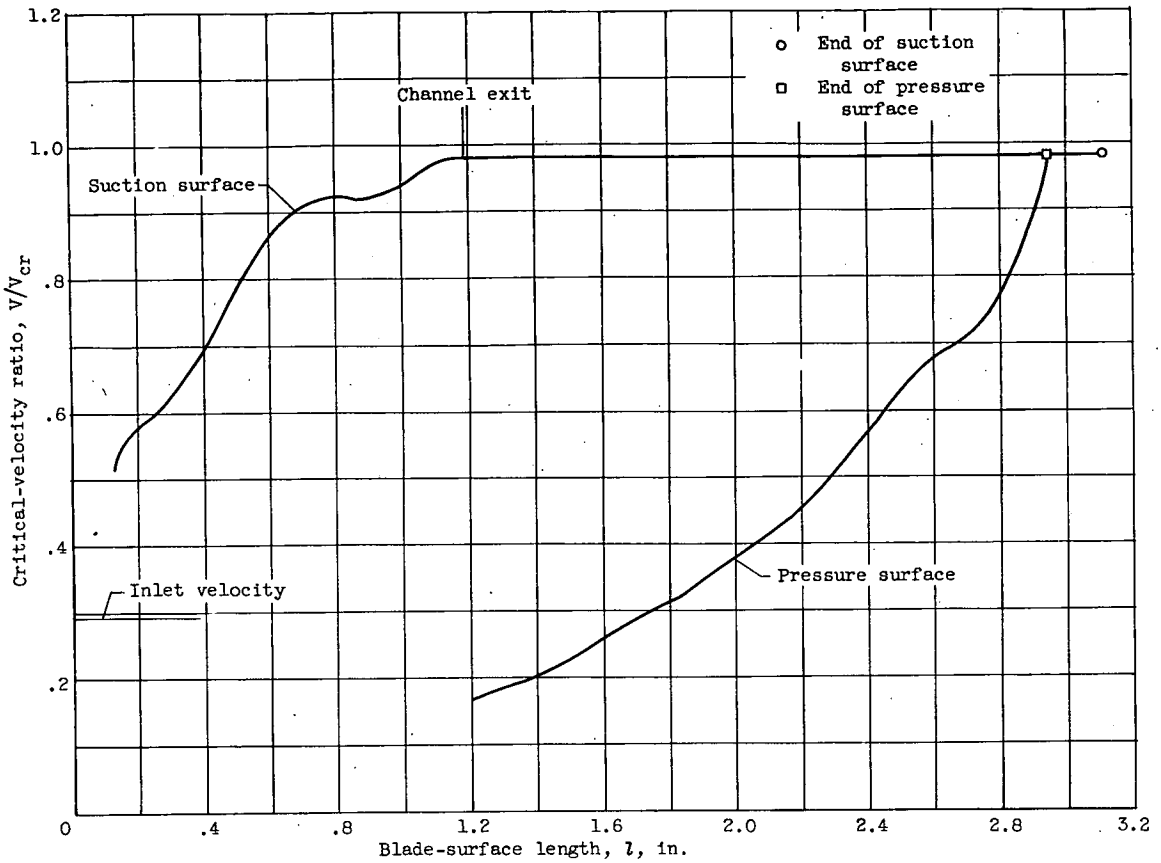

(c) Tip.

Figure 3. - Concluded. Design stator-surface velocity distributions at hub, mean, and tip sections.

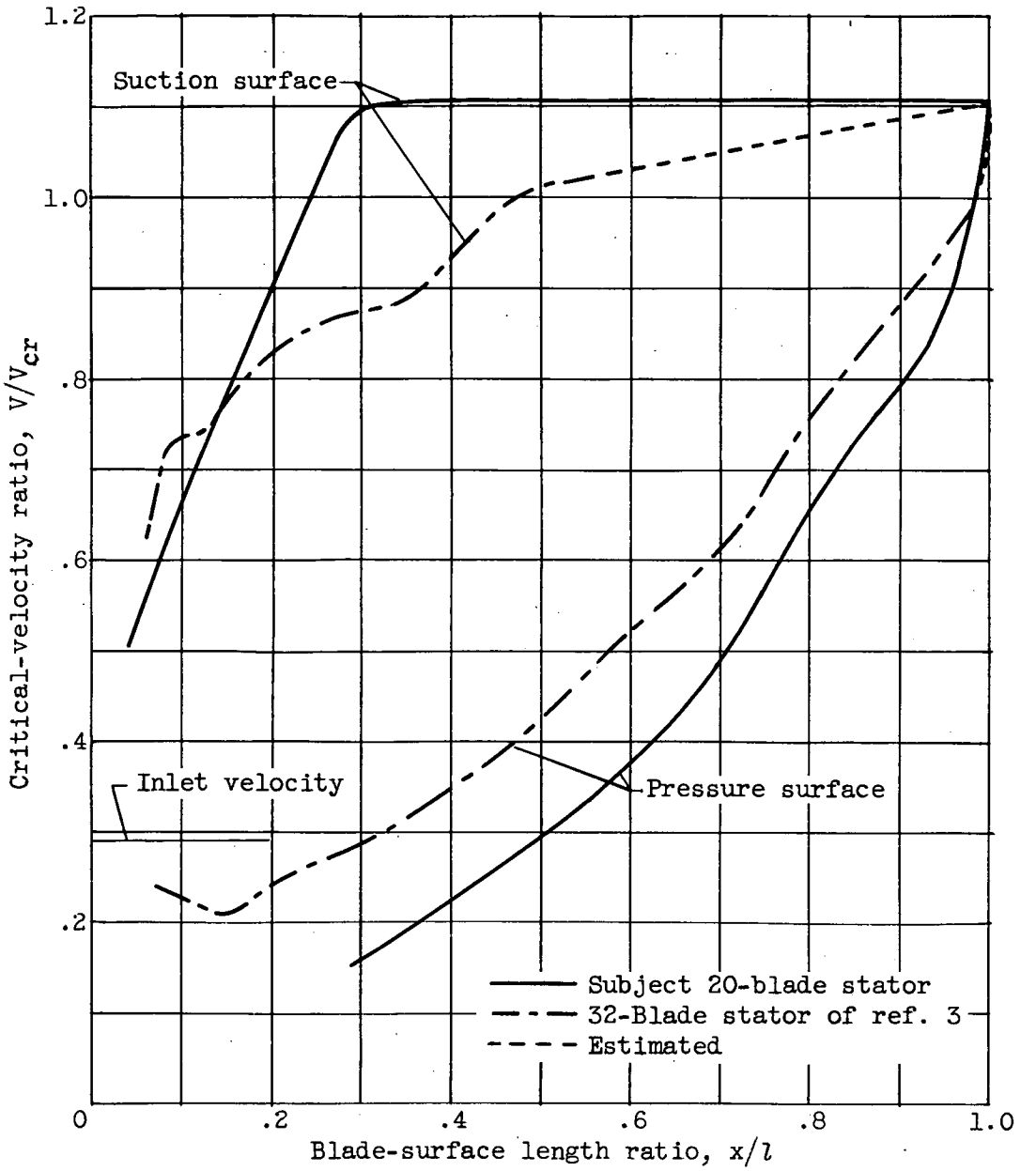

Figure 4. - Design surface velocity distributions at mean section for subject stator and stator of reference 3.

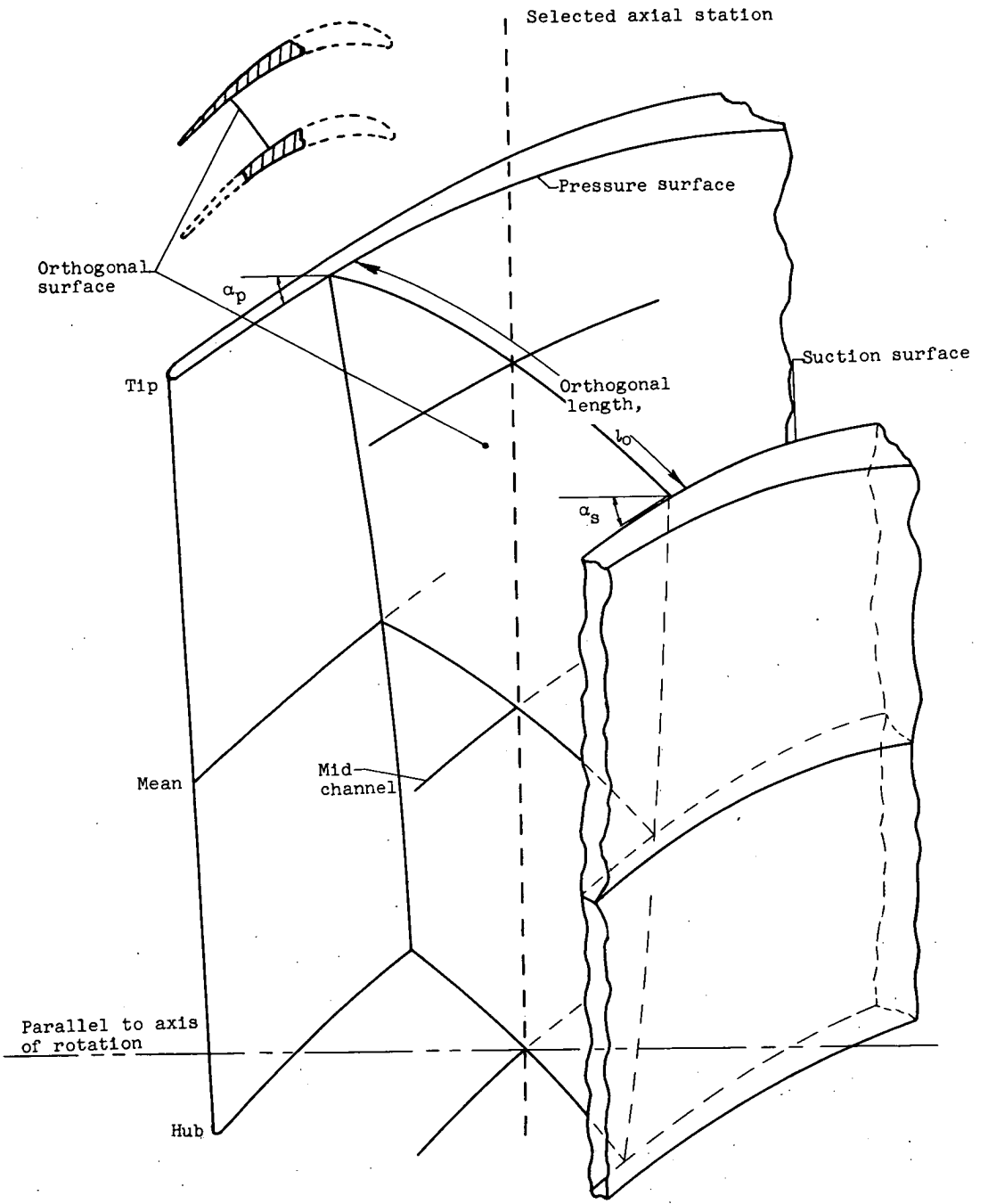

Figure 5. - Description of orthogonal surface and some variables in design procedure.

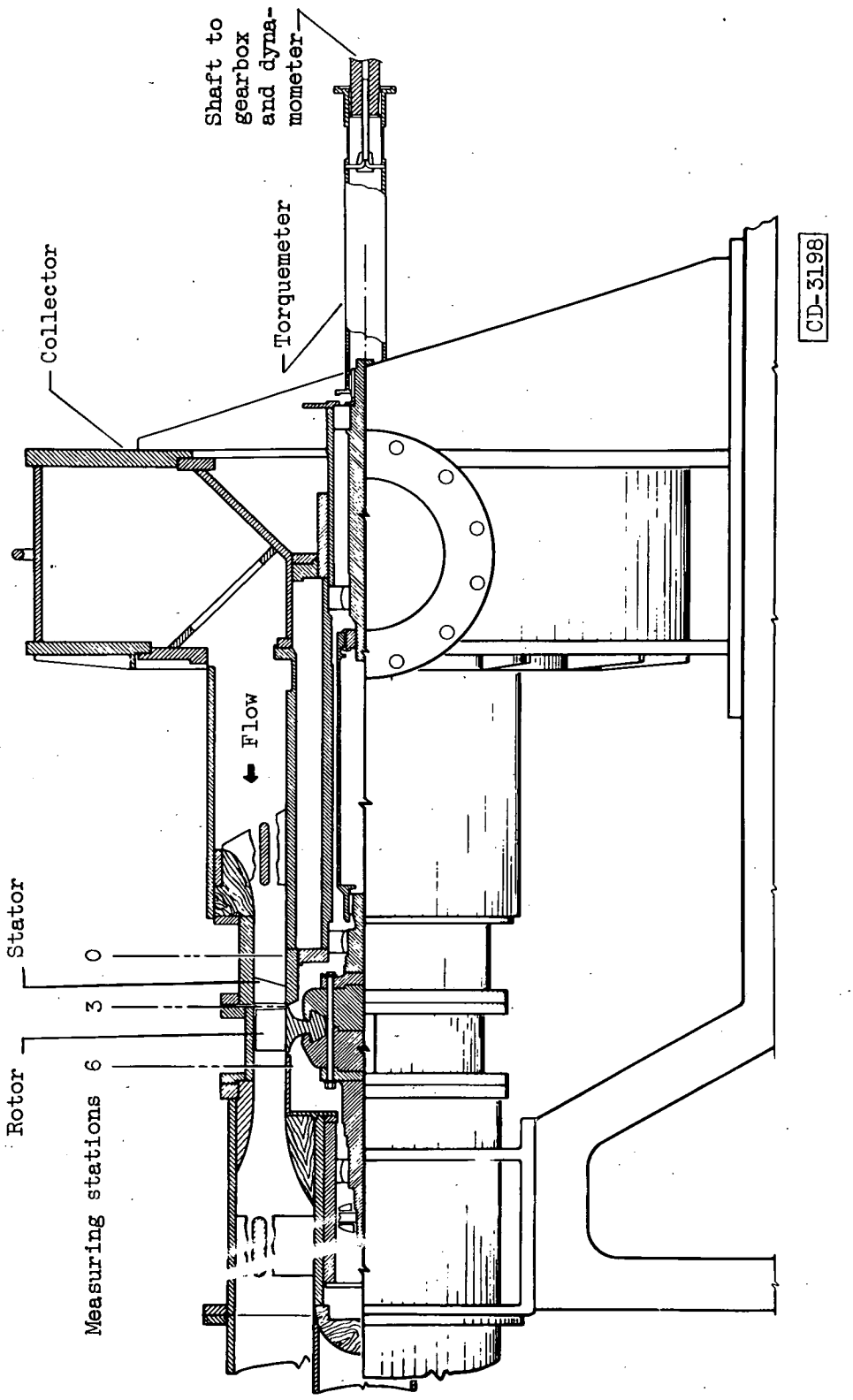

Figure 6. - Diagrammatic sketch of cold-air turbine test section.

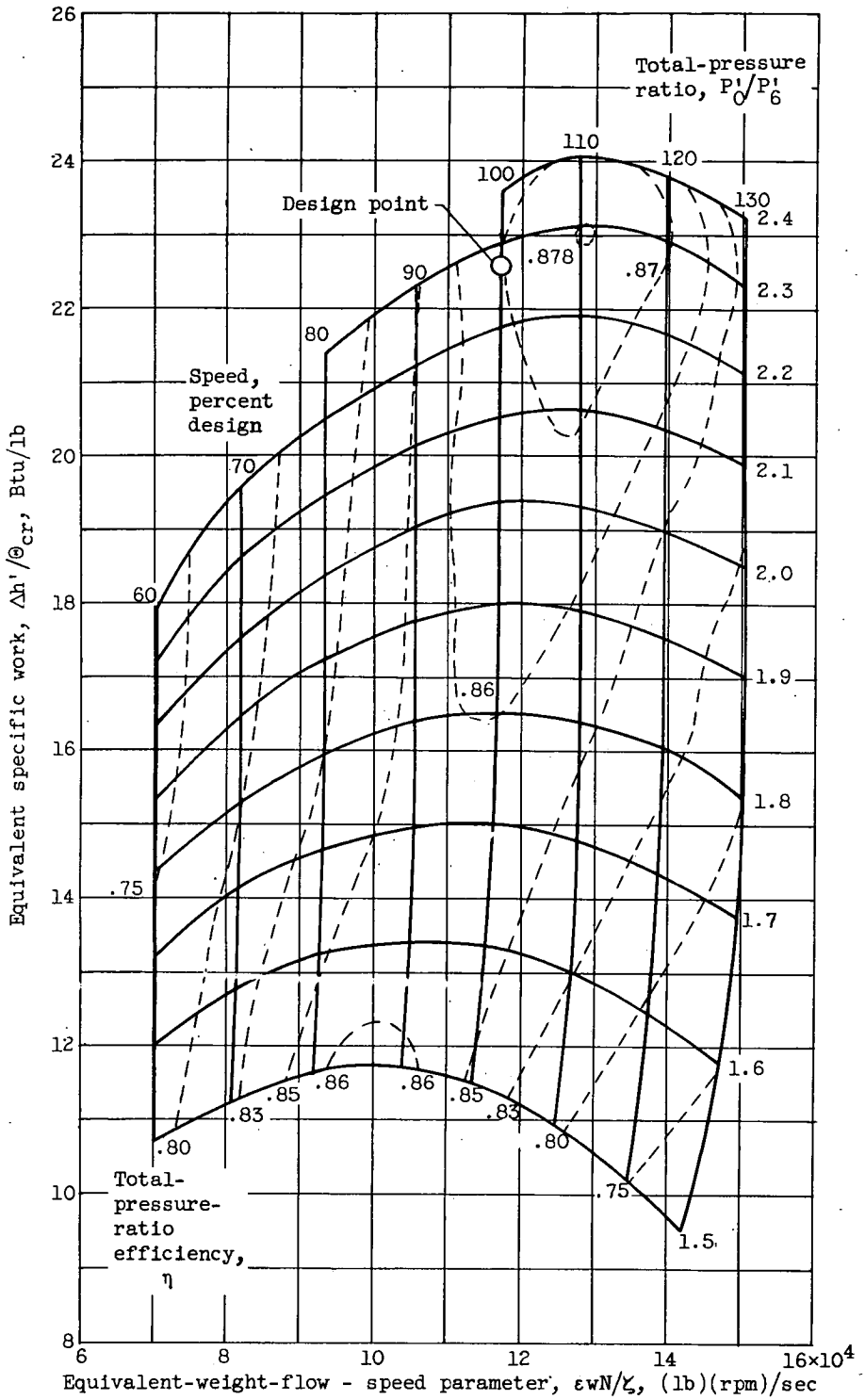

Figure 7. - Experimentally obtained performance map based on total-pressure ratio across turbine.

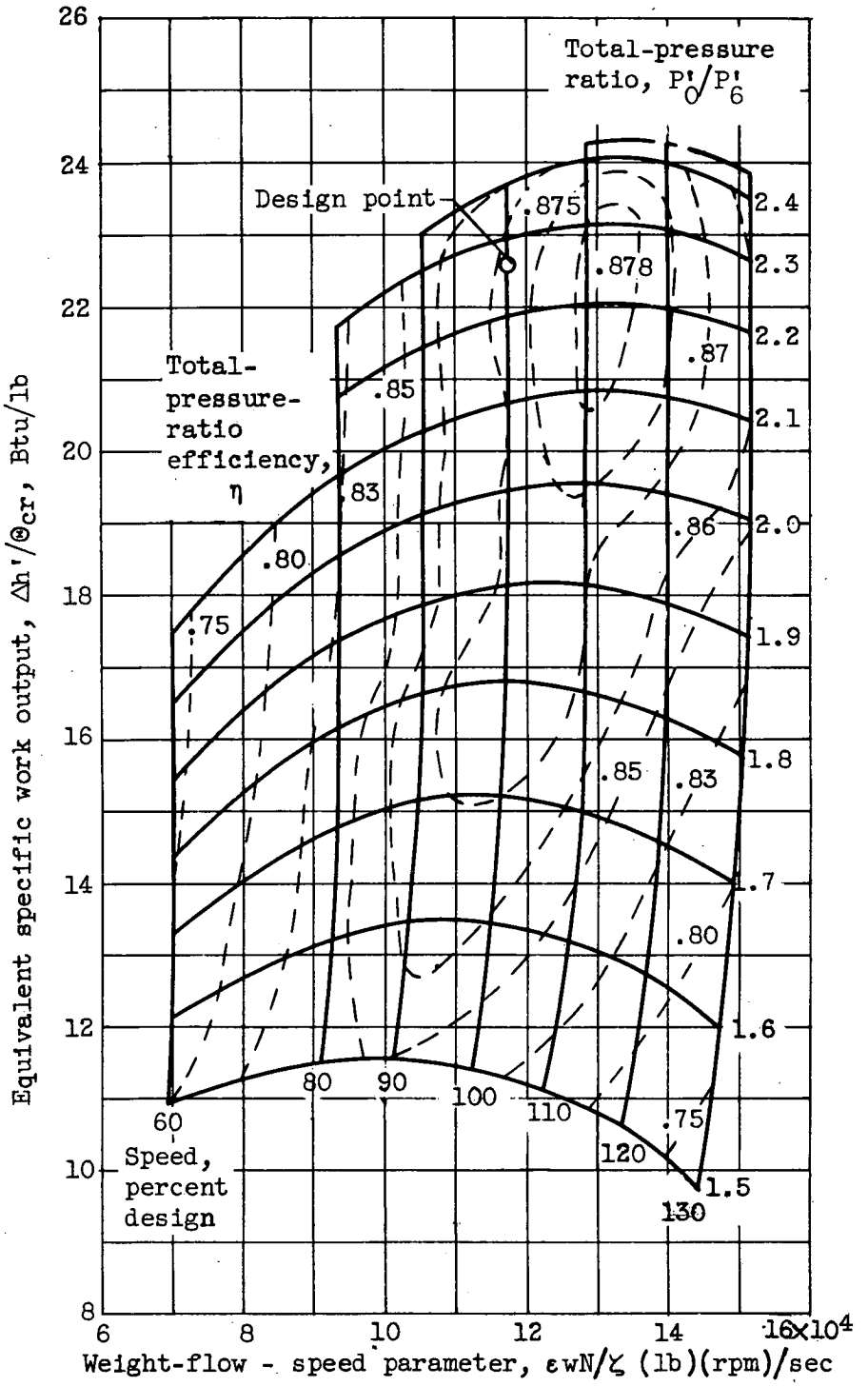

Figure 8. - Performance map based on total-pressure ratio for turbine of reference 3.

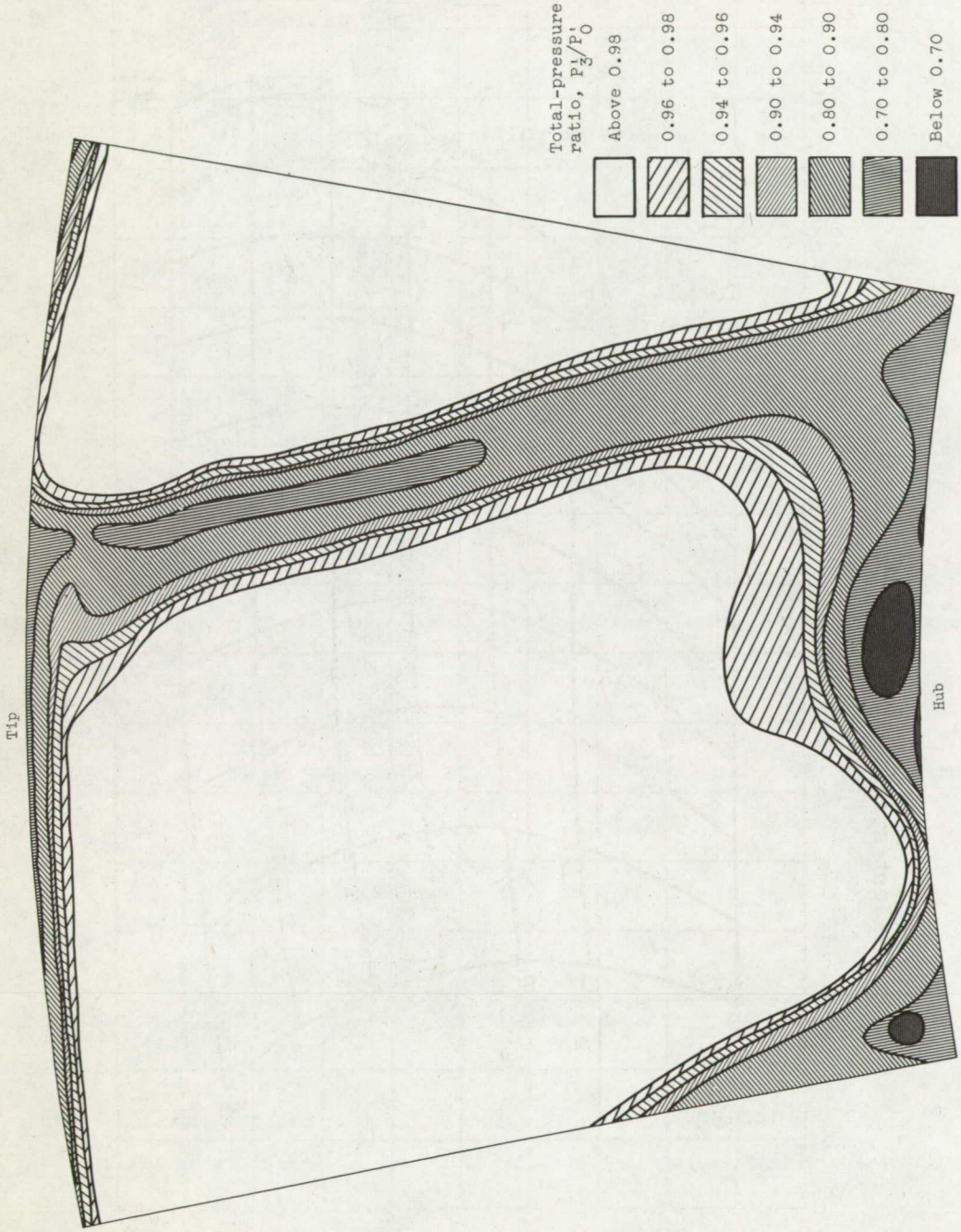

Figure 9. - Contours of total-pressure ratio from detailed surveys near stator trailing edge at design conditions. (Portion of turbine-outlet flow annulus shown corresponds to about $1\frac{1}{4}$ stator passages.)

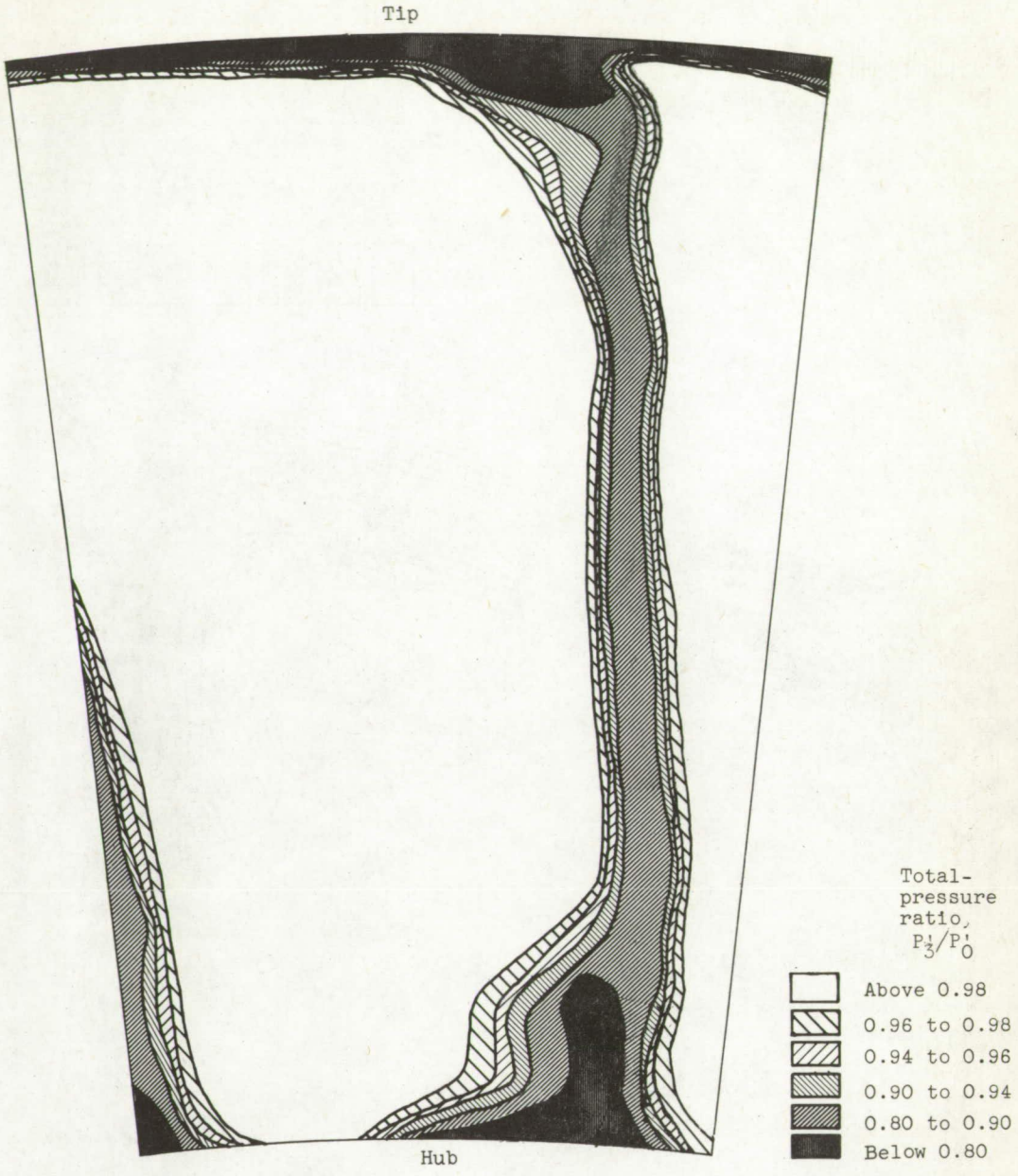

Figure 10. - Contours of total-pressure ratio from detailed surveys near the stator trailing edge at design pressure ratio across stator for stator of reference 3. (Portion of turbine-outlet flow annulus shown corresponds to about $1\frac{1}{4}$ stator passages.)

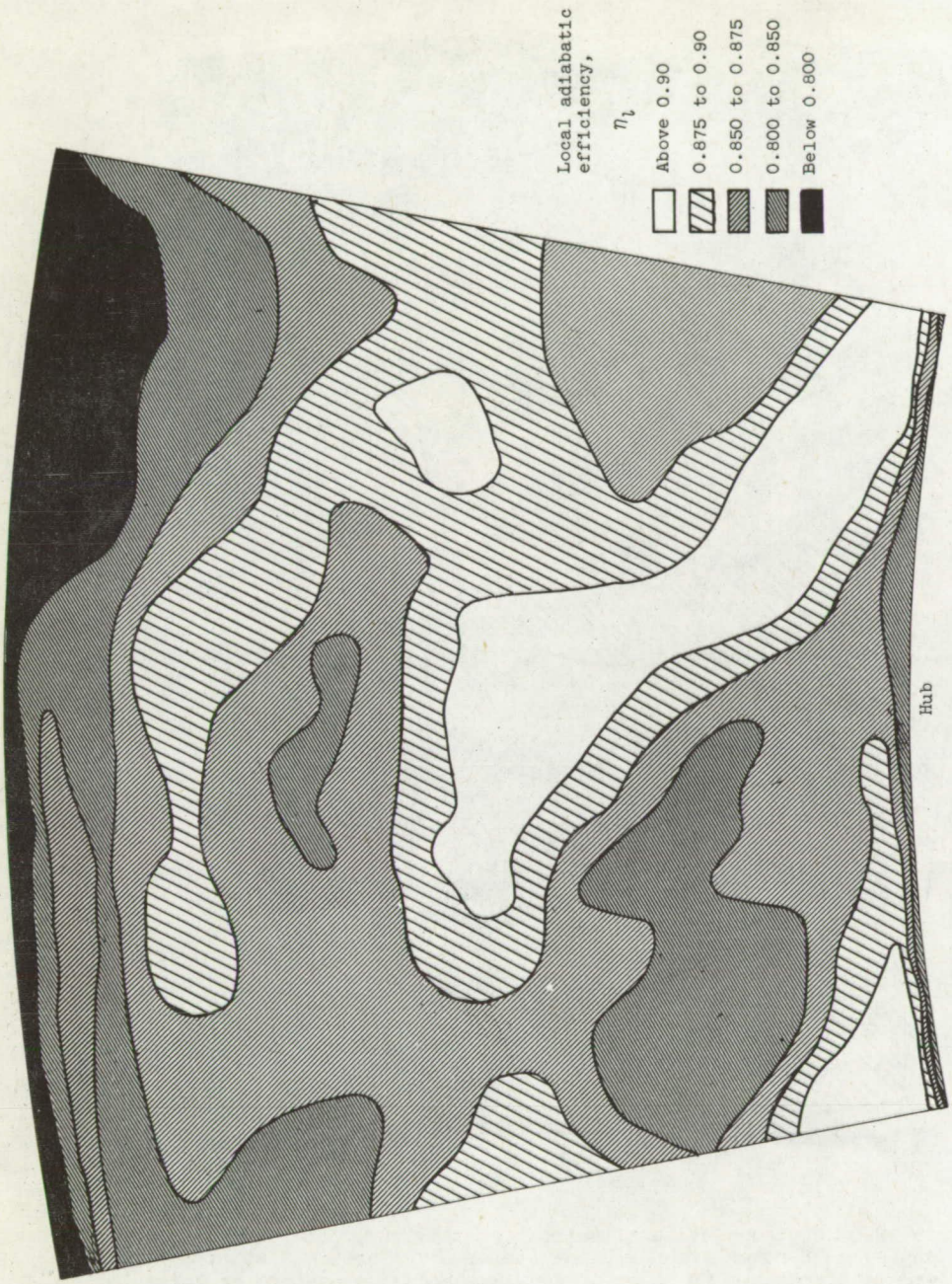

Figure 11. - Contours of local adiabatic efficiency from detailed surveys downstream of rotor at design operating conditions. (Portion of turbine-outlet flow annulus shown corresponds to about $1\frac{1}{4}$ stator passages.)

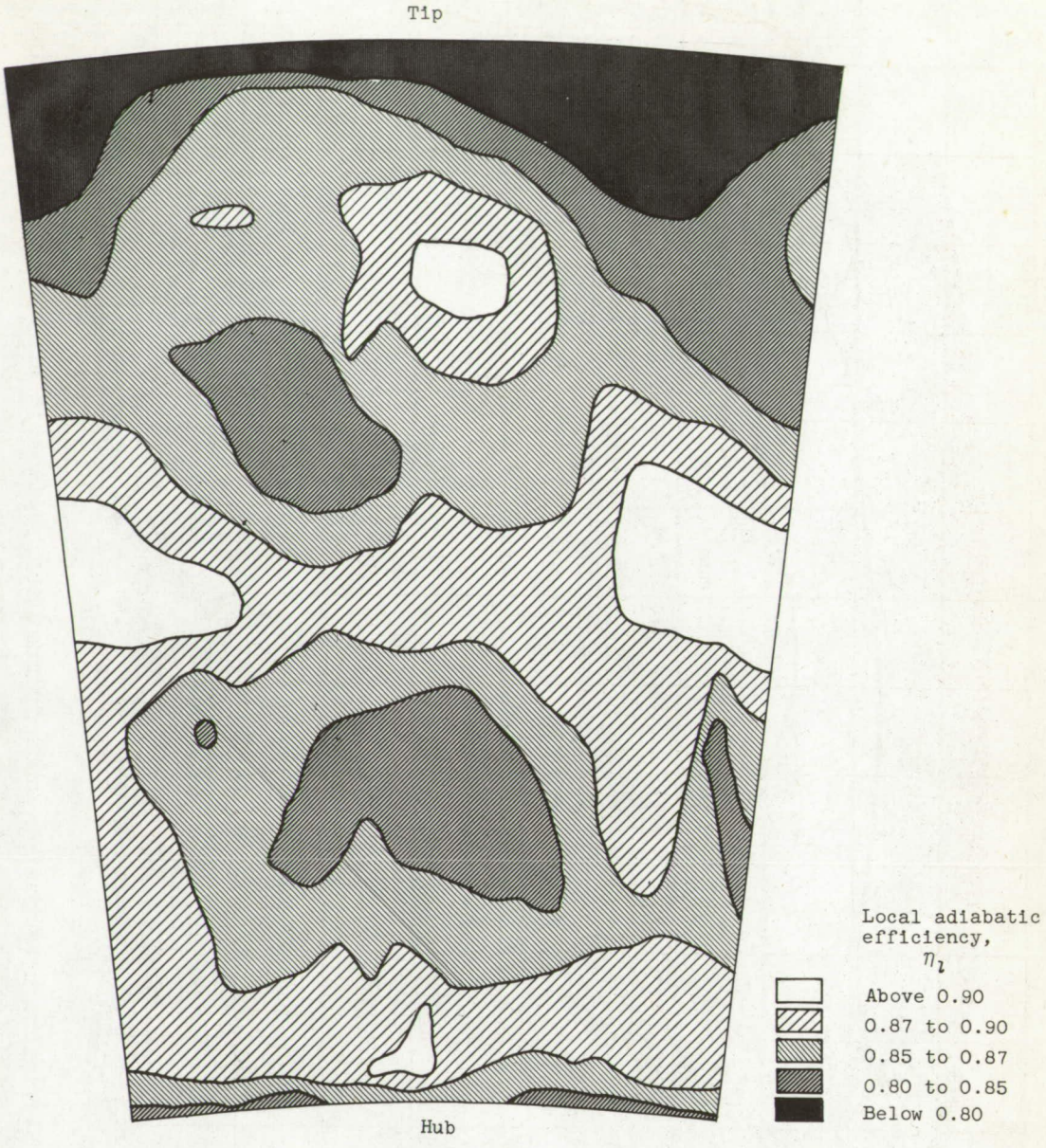

Figure 12. - Contours of local adiabatic efficiency from detailed surveys downstream of rotor with 32-blade stator of reference 3 at approximately design conditions. (Portion of annulus shown corresponds to about $1\frac{1}{4}$ stator passages.)

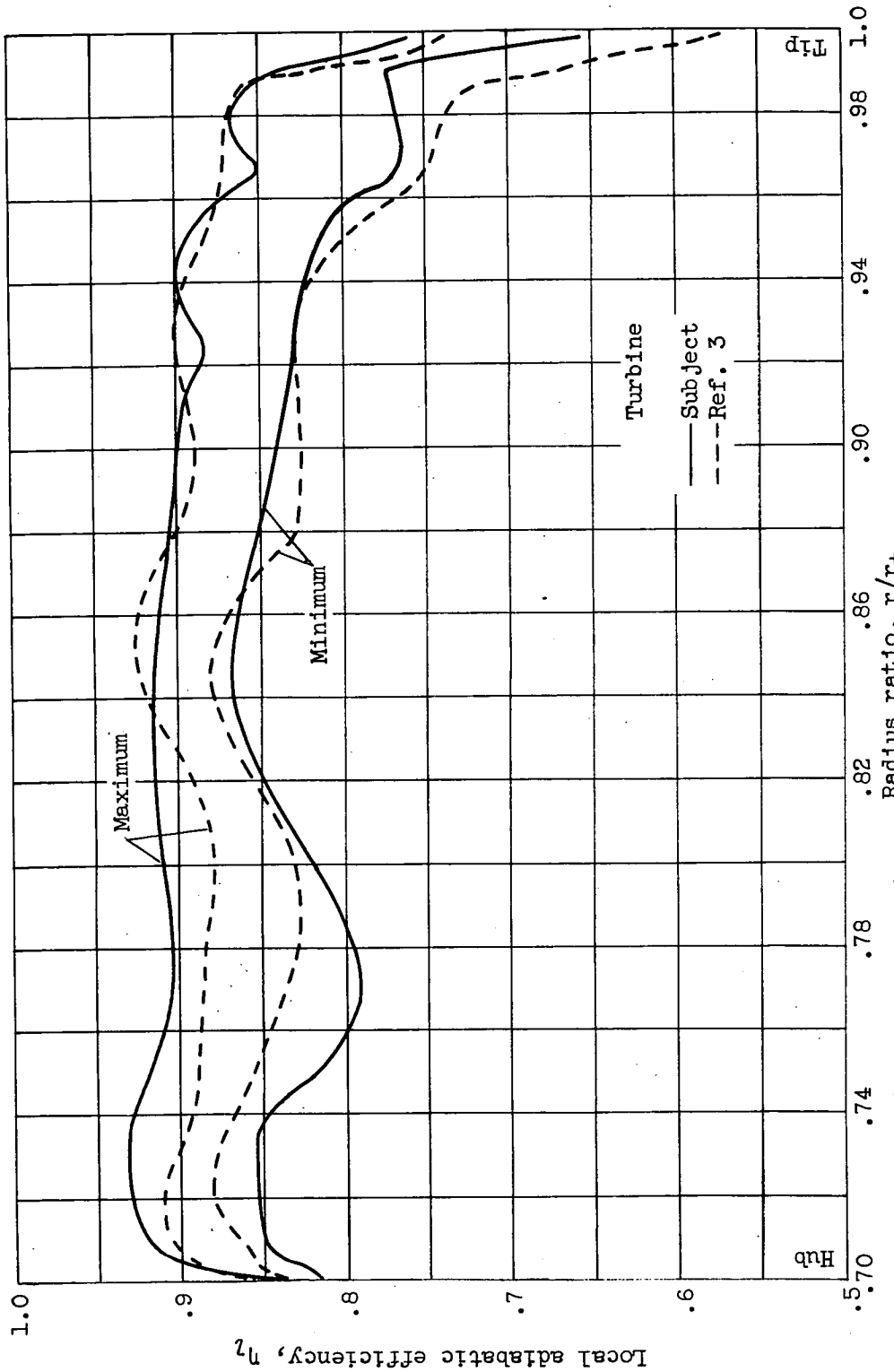

Figure 13. - Variation of maximum and minimum local adiabatic efficiencies with radius ratio.

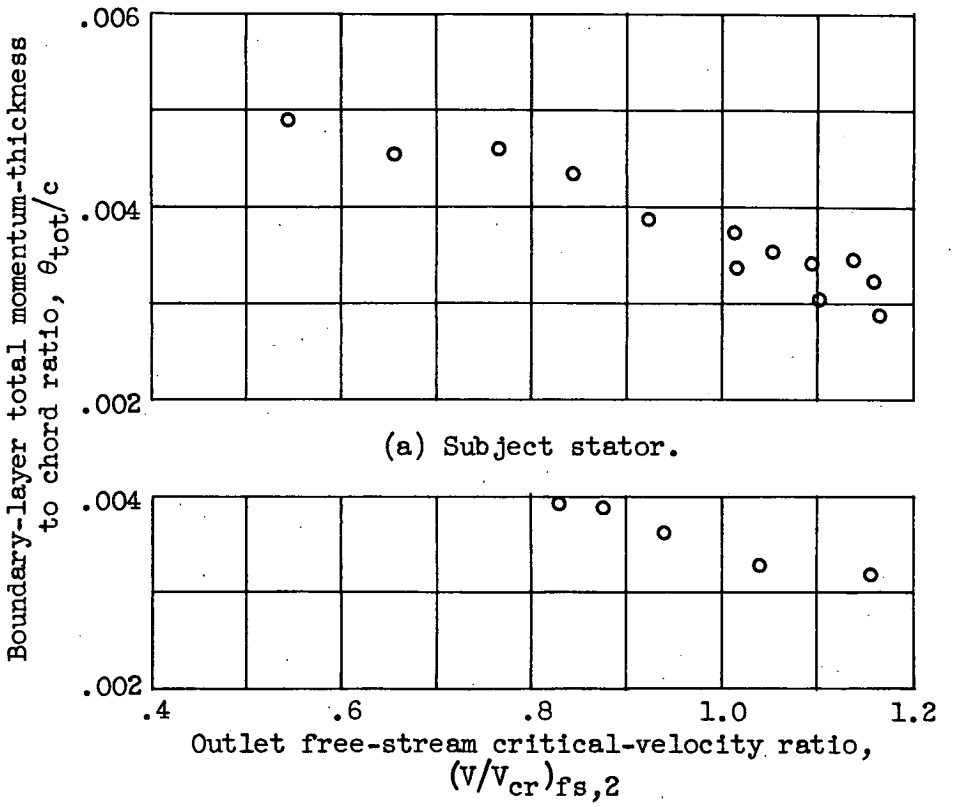

(b) 32-Blade stator of reference 3.

Figure 14. - Total momentum-thickness to chord ratio as function of outlet free-stream critical-velocity ratio based on total-pressure surveys at mean-section trailing edge.

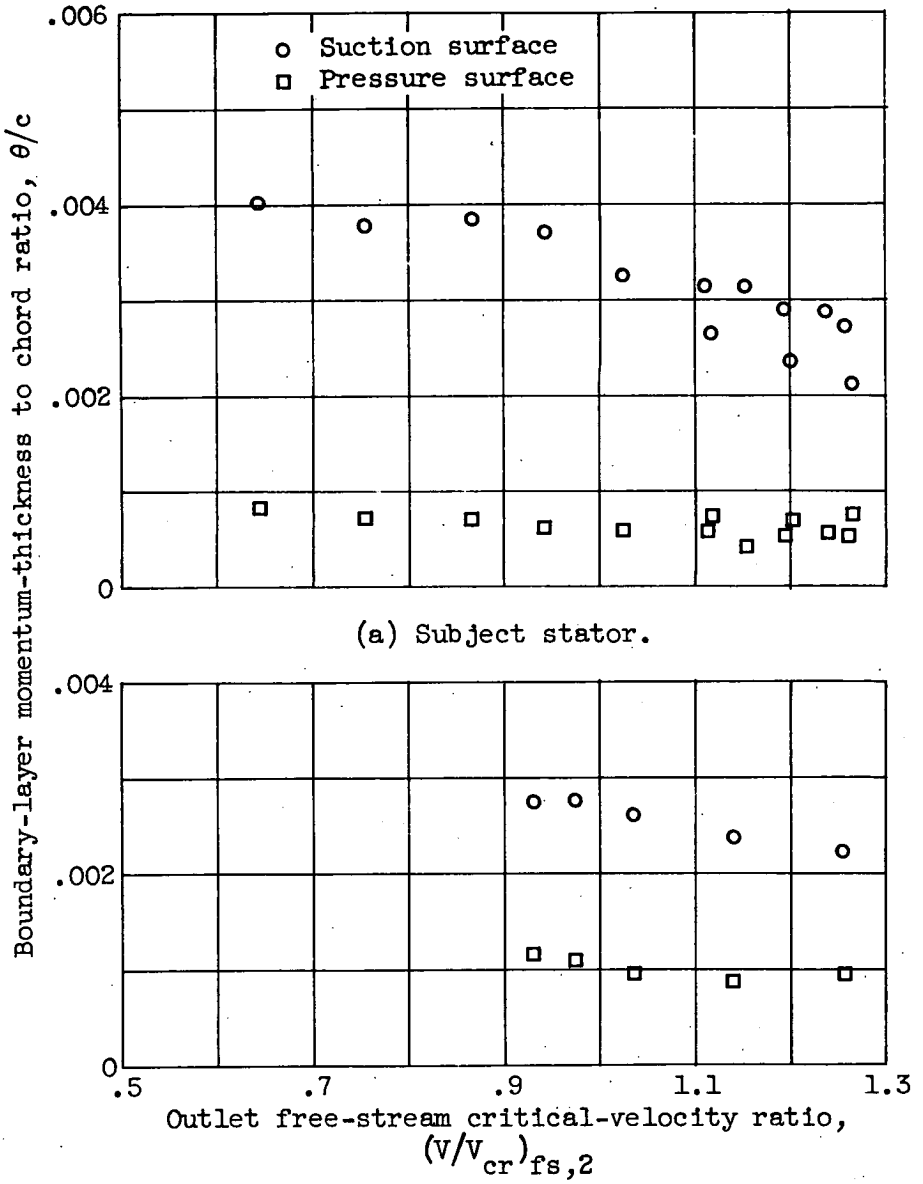

(a) Subject stator.

(b) 32-Blade stator of reference 3.

Figure 15. - Transonic-turbine stator surface momentum-thickness to chord ratio as function of outlet free-stream critical-velocity ratio.

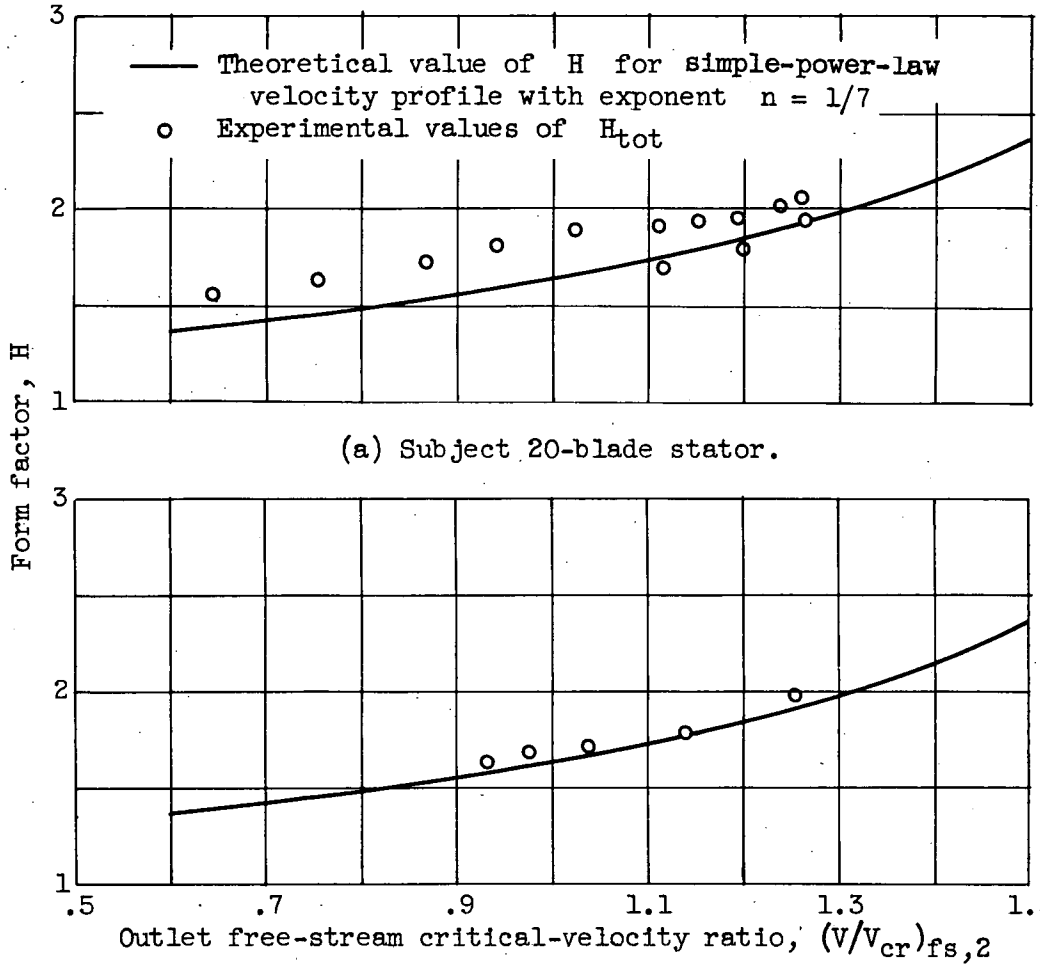

(a) Subject 20-blade stator.

(b) 32-Blade stator of reference 3.

Figure 16. - Variation in wake form factor with outlet free-stream critical-velocity ratio obtained from surveys behind two transonic-turbine stators.

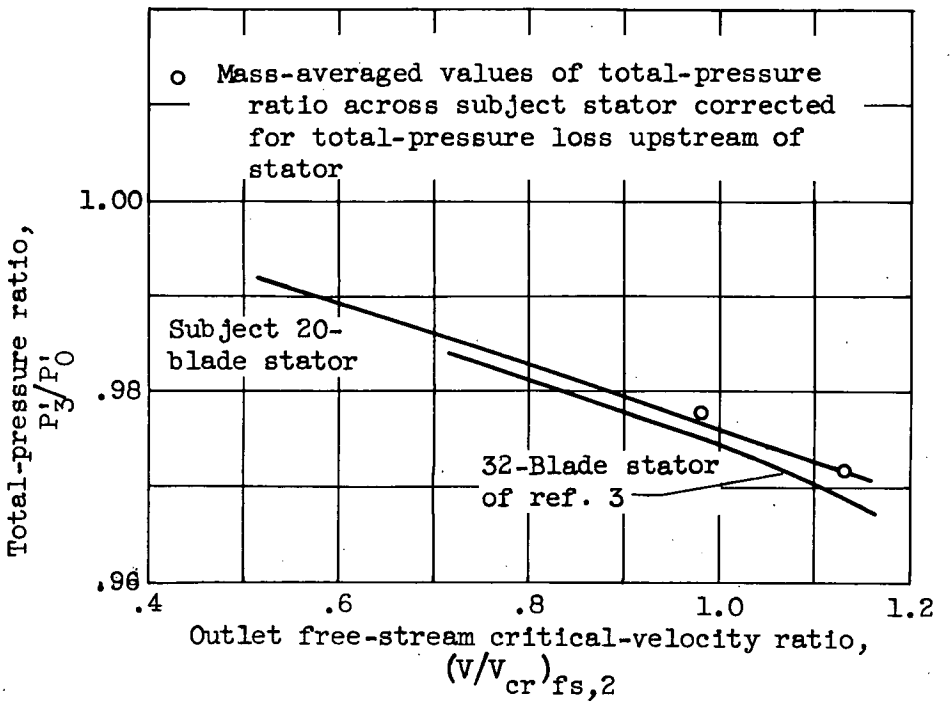

Figure 17. - Variation in total-pressure ratio across stator with blade-outlet critical-velocity ratio based on experimental values of momentum thickness at mean-section trailing edge.

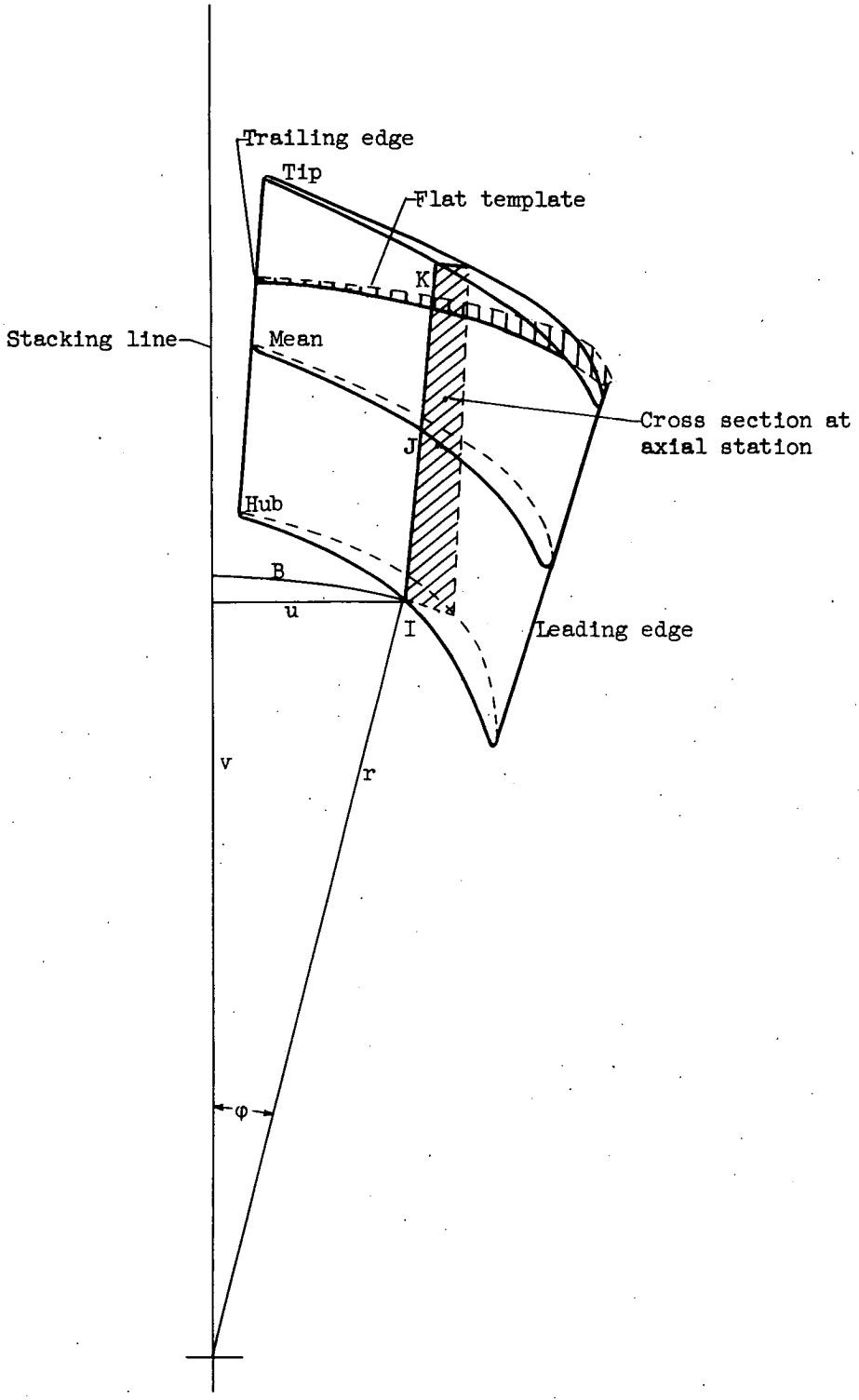

Figure 18. - Cylindrical and Cartesian coordinates of a point on a radial plane through a three-dimensional blade.